CO organization at ambient pressure on stepped Pt surfaces: First principle modeling accelerated by neural networks

Vaidish Sumaria† and Philippe Sautet*,†,‡

†*Department of Chemical and Biomolecular Engineering, University of California, Los Angeles, CA 90094, USA*

‡*Department of Chemistry and Biochemistry, University of California, Los Angeles, CA 90094, USA*

E-mail: sautet@ucla.edu

Abstract

Step and kink sites at Pt surfaces have a crucial importance in catalysis. We employ high dimensional neural network potential (HDNNP) trained using first-principle calculations to determine the adsorption structure of CO in ambient conditions (T=300 K, P=1 atm) on these surfaces. To thoroughly explore the potential energy surface (PES), we use a modified Basin Hopping method. We utilize the explored PES to identify the adsorbate structures and show that in the considered conditions several low free energy structures exist. In the considered temperature and pressure conditions, the step edge (or kink) is totally occupied by on-top CO molecules. We show that the step structure and the structure of CO molecules on the step dictate the arrangement of CO molecules on the lower terrace. On surfaces with (111) steps, like Pt(553), CO forms quasi-hexagonal structures on the terrace with the top site preferred, with in average two top sites CO for one multiply bonded CO, while in contrast surfaces with (100)

steps, like Pt(557), present a majority of multiply bonded CO on their terrace. Short terraced surfaces like Pt(643), with square (100) steps that are broken by kink sites constrain the CO arrangement parallel to the step edge. Overall, this effort provides detailed analysis on the influence of step edge structure, kink sites, and terrace width on the organization of CO molecules on non-reconstructed stepped surfaces, yielding initial structures for understanding restructuring events driven by CO at high coverages and ambient pressure.

1 Introduction

The active phase of transition metal heterogeneous catalysts present atoms in different coordinations and environments. Surface science experiments over the last two decades have systematically studied the relation between surface structure and catalytic activity by using single-crystal surfaces as model catalysts. Open surface structures or surfaces with high Miller index often show enhanced activity.[1–5] The high-index planes, denoted by a set of Miller indices (hkl) with at least one index being larger than one have a high density of atomic steps and kinks. The low coordination atoms which define the atomic step/kink sites on the catalyst surface often enable enhanced binding of reactant molecules and exhibit higher activity for bond breaking.[6–13] At the same time, steps also play an important role in other surface processes like adsorbate induced reconstructions. The surface atoms at the step/kink site act as a natural locations for crystal growth and erosion; and as a source for mobile surface ad-atoms during the process of surface reconstruction.[14–19] This makes it important to study the assembly structure of adsorbate molecules on such stepped surfaces in realistic temperature and pressure conditions (which defines the adsorbate chemical potential) to understand the adsorption site distribution and the adsorbate coverage. Such a high coverage adsorbate structure is the initial configuration for adsorbate induced surface reconstruction processes at such stepped and kink surface sites. In this work, we focus our attention on the Pt/CO system to understand the CO organization on Pt(553), Pt(557) and

Pt(643) surfaces at room temperature and ambient pressure. All these surfaces show (111) terraces, separated by (111) and (100) mono-atomic steps for Pt(553) and Pt(557) respectively. Pt(643) is a case where the step includes kinks, hence presenting Pt atoms with a metallic coordination of 6.

Since the considered step surfaces all present (111) terraces, the behavior and organization of CO on the extended Pt(111) surface is a key reference. CO adopts on Pt(111) multiple ordered structures depending on the coverage. At 300 K and 1 atm pressure of CO, experiments (as scanning tunneling microscopy) and first principle modelling show that CO molecules adopt a so called "Moiré pattern" structure, in which CO, binding vertically through the C atom, is organized in a pseudo-hexagonal layer with a rotated supercell with respect to the underlying 1x1 hexagonal Pt layer. More specifically a $(\sqrt{19}\times\sqrt{19})$-$R23.4°$-13 CO unit cell is found where 13 CO molecules occupy a cell containing 19 Pt atoms, corresponding to a coverage of 13/19 = 0.68 ML (see SI S4).[20–23] Since the CO quasi-hexagonal layer has a slightly larger parameter than that of the Pt(111) layer, CO molecules span a variety of binding sites, from (quasi) top to bridge and hollow. Although the classification between these various sites relies on chosen thresholds and hence is somewhat ambiguous, one can determine that, among the 13 CO molecules, 7 are in a top or quasi top site, while 4 in bridge/ quasi-bridge and 2 in hollow sites. So about one half CO molecules are on the top site, while the other half is in a multiply bonded site. Many experiments are performed in UHV conditions with a small CO pressure and low temperature to reach a high CO coverage. In these conditions, the CO coverage is typically somewhat lower (0.5 ML) and a simple c(4x2)-2CO superstructure is seen, with one top and one bridge CO. Hence, a very similar ratio (0.5) is seen between top and multiply bonded CO, compared to the high pressure Moiré pattern arrangement.

If we now move to stepped and kinked surfaces, the experimental characterization of adsorbate layers surfaces is challenging. These surfaces are heterogeneous, with different types of sites (step, kink, terrace), and adsorption is usually less ordered. For example,

Tränkenschuh et al. did not find any LEED pattern for CO adsorption on Pt(553), showing an absence of long range order, in contrast to Pt(111).[24] This absence of long range order was also seen on many other high index surfaces (Pt(533)[25], Pt(332)[26], Pt(210)[27] and Pt(321).[28] Spectroscopic characterization methods necessarily give space average information. For CO on stepped Pt surfaces, high resolution X-ray photoelectron spectroscopy (XPS) and electron energy loss spectroscopy (EELS) can distinguish between CO adsorbed at step sites and terrace sites, and between top and bridge bonded CO at each site.[15,24,26,29–31] On Pt(553), XPS at low pressure (less than 3×10^{-9} mbar) and low temperature (130K) shows that the terrace is only occupied when the edge sites are almost saturated with CO, while on the terrace the population of the top site is about twice that of the bridge site at saturation coverage of ~0.5 ML.[24] This contrasts with the case of Pt(111) where at a similar coverage the population of top sites equals that of bridge sites. On Pt(335) at 0.5 ML coverage, EELS also shows that all edge sites are occupied with top CO, while on the terrace half of the sites are occupied with a 2:1 top-to-bridge ratio.[26]

In situ FTIR studies in solution and electrochemical conditions indicates that the preferred binding mode of CO on the terrace of stepped surfaces with short terraces depends on the type of step: surfaces with (100) steps (Pt(322) and Pt(311)) show a large amount of bridge site CO on their terraces, while those with (111) steps (Pt(332) and Pt(331)) mostly provide top site CO.[32] This suggests an interesting mechanism, of unknown origin to our knowledge, by which the type of step can control the binding site of CO on the terraces. Near-Field microscopies, such as scanning tunneling microscopy, provide images with molecular resolution, but the detailed interpretation of the images can be challenging, and time resolution is usually limited. STM images of 0.5 ML of CO on a Pt(111) surface presenting steps shows less order and higher mobility of CO molecules in the vicinity of the step.[33]

Computational studies that investigate high Miller index surfaces with high adsorbate coverage are very limited. The complexity of modeling such surfaces arises from two major challenges: (1) the high computational cost of exploring such potential energy surface (PES)

using accurate first principles calculations and (2) the myriad combinations of adsorption sites possible at high coverages. To tackle the first challenge, we use the approach developed by Behler and Parrinello to generate a High Dimensional Neural Network Potential (HDNNP)[34] that is trained on higher-level first principles calculations and can accurately describe the adsorbate–adsorbate and adsorbate–surface interactions on various high Miller surfaces. This approach is ideal for studying these systems because it scales favorably with respect to the dimensionality of the system and guarantees the permutation invariance of the PES due to the conversion of unique local environments into unique fingerprints. In the past few years, NN based methods have been increasingly used to construct such accurate PES successfully.[35–43] To tackle the second challenge of exploring the large combination of adsorption sites possible, we use a Basin-hopping algorithm.[44] This method transforms the PES into local minima basins and the transition between these basins is accomplished by performing a Monte-Carlo displacement trial move, followed by geometry optimization. Such a method is not very often applied while using DFT to compute the free energy of the system to evaluate the MC criteria due to the high cost of DFT calculations and due to the fact that a significantly high number of MC steps can be required to reach a global minimum. Having an accurate and quick energy calculator in terms of the HDNNP, we can efficiently generate a large number of configurations of CO on different Pt surfaces for a given coverage and chemical potential of CO.

In most theoretical studies, the PES is not thoroughly sampled and only a few local minima are found, the most stable one being supposed to represent the structure of the adsorbates on the substrate. This is due to the unaffordable cost of modeling and exploring the PES as we discussed before. However, it is now known that the pressure of the adsorbates can generate dynamic interfaces which can play a nontrivial role in understanding the actual distribution of the adsorbates on the surface. The majority of the discussion of such dynamic states in the literature has been focused on understanding the fluxionality of small nanoparticles and nanostructured surfaces.[45–50]. Sun et al., discussed the case of a Pt_{13} cluster under

a pressure of hydrogen, found a large ensemble of low energy structures, and showed that these structures change with hydrogen coverage. Metastable structures are shown to dominate the catalytic activity. One observation made in the case of $Pt_{13}H_{26}$ structures was that all the structures in the metastable ensemble exhibited a cuboctahedral Pt_{13} core, and the only variation in the structures was produced by the hydrogen atoms occupying different positions on the cluster. This indicates that metastable structures can be generated by just rearrangement of adsorbate atoms and hence that the concept of metastable ensembles can also be applied to a gas-surface interaction. In this work, using basin hopping simulations, we not only search for the global minima for CO adsorption structures on various stepped surfaces, but also find the coverage dependent ensemble of possible CO configurations. We show that the CO organization on the terrace are strongly affected by the geometry of the step ((100) or (111) facets), which controls the ratio between top and multiply-bonded CO molecules, that quasi-hexagonal CO lattices are formed on these terraces similarly to the case of Pt(111)[17,21] and that step edges are in most cases fully covered with one top site CO molecule on each step Pt atom.

2 Results and Discussion

2.1 Pt(553)

Pt(553) can be represented as Pt(S)-[5(111) × (111)] in step notation since it is formed by a 5 atom wide Pt(111) terrace followed by a mono-atomic 111-type step as shown in Fig. 1(a) and (b). One challenge is that no long-range order for CO is found experimentally on such stepped surfaces, while a unit cell is required to model the surface. We tackle this by considering several unit cells, that describe a rather large area of the step and terrace. This is possible only because we obtain a fast and accurate neural network potential enabling to sample a very large number of configurations for CO molecules, at variable coverage, on these unit cells. Such a sampling would be extremely computationally costly using DFT

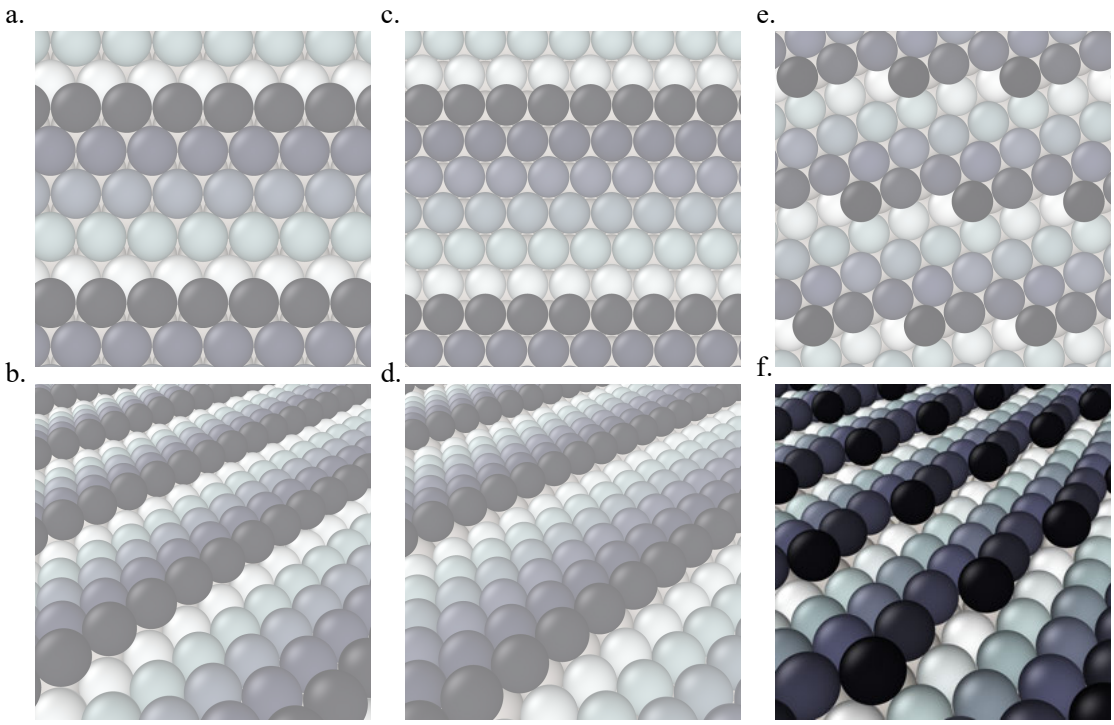

Figure 1: Ball Models of various clean surfaces considered. (a) Pt(553) top view, (b) Pt(553) side view, (c) Pt(557) top view, (d) Pt(557) side view, (e) Pt(643) top view, Pt(643) side view. Colors represent the z-position of the atoms. Black balls represent the step edge and others represent the terrace.

calculations. For Pt(553) we use 3x1, 4x1, 6x1 unit cells, with the first periodic direction being along the step edge while the second one (x1) corresponds to the (long) periodicity between one step and the next one. With these unit cells, we can explore the various organisation periodicities of molecules along the step edge using basin hopping simulations.

We calculate the total Gibbs free energy of adsorption for all CO molecules, including entropy terms for the gas phase molecules but neglecting the vibrational entropy for adsorbed molecules. This adsorption energy is then normalized to a 1 $Å^2$ surface area, to be able to compare different unit cells. Fig. 2(a) shows the Gibbs adsorption free energy of CO per unit surface area on Pt(553) as a function of CO coverage. A total number of 1501 local minima configurations have been explored, and their free energy is shown by dashed lines in fig 2a, the orange lines (97 structures) representing the low energy accessible region, called here the low energy metastable ensemble (LEME). The energy interval for the LEME is chosen to 1

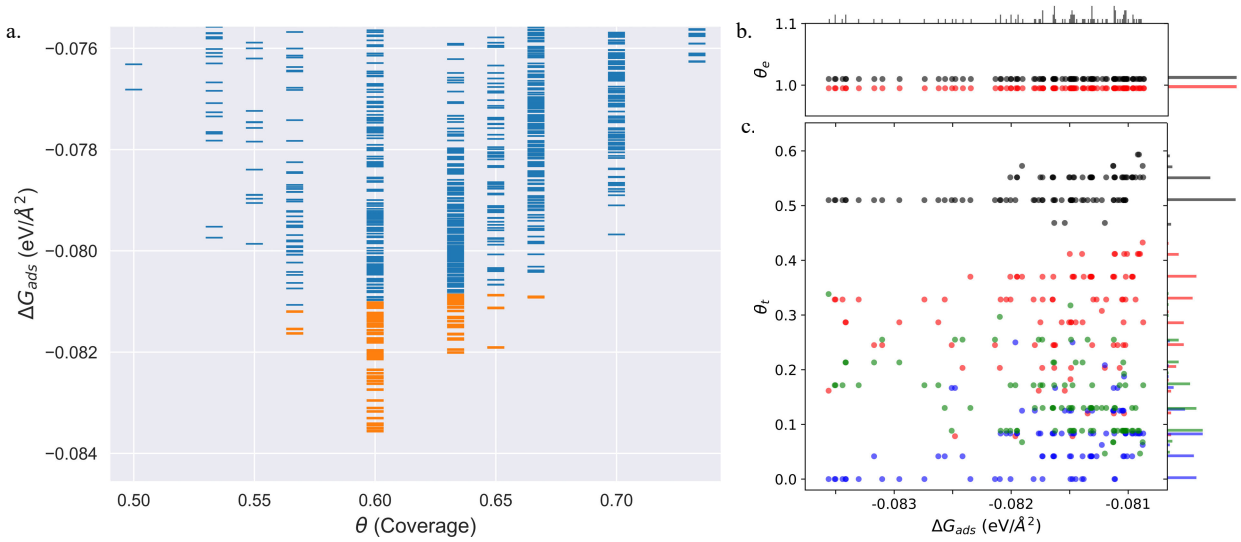

Figure 2: (a) Adsorption free energy per unit surface area ΔG_{ads} (at T=300K, P=1 atm) plotted against CO coverage (θ) on Pt(553). Yellow markers represents the structures defending the Low energy minima ensemble. (b) and (c) represent the coverage of CO on the Pt step-edge and terrace as a function of the ΔG_{ads} respectively. ● represents top site, ● represents bridge site, ● represents hollow site and ● represents the total coverage. The density of different sites at various coverages is represented by the histogram attached to the right ordinate axis. The density of structures as a function of ΔG_{ads} is represented by the histogram on the top abscissas axis. In plots (b) and (c), to distinguish the points, we move the red points (top sites) on the y-axis by -0.005, green points (hollow sites) have been moved by +0.005 and black points (total coverage) have be moved by +0.01.

kT per CO adsorbate. The LEME found on the Pt(553) surface consists of structures with a coverage between θ =0.55 and θ =0.67. So the first clear comment is that we do not find a single stable structure, and CO coverage for the considered T,P conditions, but in contrast, a large number of competing low energy structures are seen corresponding to a range of coverage. This simply explains the absence of long range order in the experiment.

Common points and differences between these 97 structures in the LEME can be seen from Fig. 2, where the coverage for various CO binding modes (top, bridge, hollow) is indicated on the step edge (Fig 2 (b)) and on the terrace (Fig 2 (c)), as a function of the adsorption free energy per unit surface area. The data used to create this plot has been included on the supporting information (see SI Table S1). All structures in the LEME have the step edge completely populated by on-top CO molecules, with one CO per Pt atom. The coverage of the terrace ranges between 0.5 and 0.6 ML, where in average on the LEME

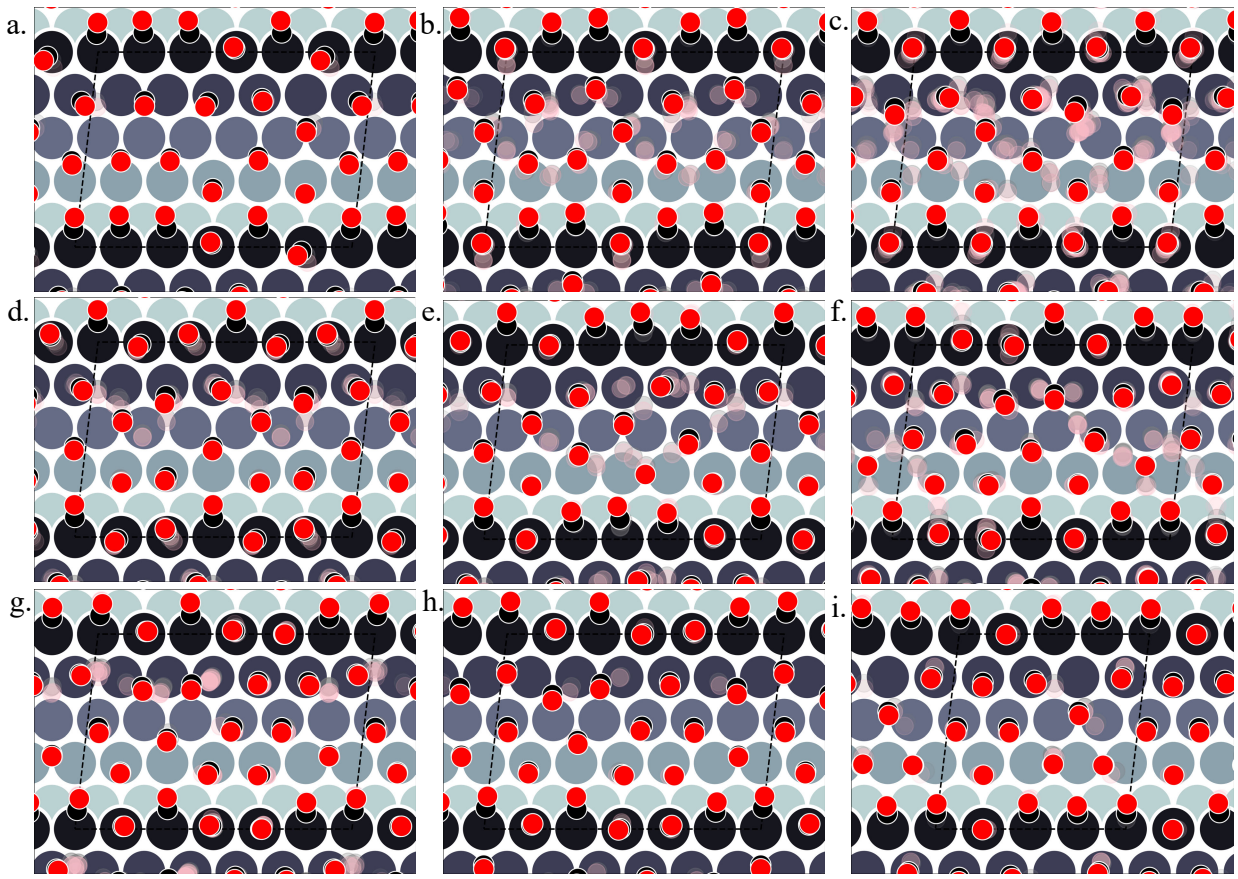

Figure 3: Various structures of CO orientations patterns observed in the LEME for Pt(553). (a) represents structures with θ = 0.56; (b)-(e) represent structures with θ = 0.6; (f)-(h) with θ = 0.63; (i) with θ = 0.65. The Pt atoms are shown using a colormap (color-bar representing z-position of the Pt atom). For a given pattern, the lowest energy orientation of CO is shown using the solid black and red balls representing the positions of C and O respectively and the ensemble of structures are represented by the "cloud" of pink and grey balls.

structures, top site occupation is dominating (average coverage 0.3 ML), followed by hollow sites (average coverage 0.14) and bridge sites (average coverage 0.07). Therefore, the amount of top CO molecules is in average about twice that of the multiply bound CO on the terrace of Pt(553).

Fig. 3(a-i) shows the structural arrangement of CO at various coverages between 0.55 and 0.67 found in LEME. For a given most stable structural arrangement of CO on the Pt(553) surface at a given coverage, small variations in the CO positions generate structures that have adsorption free energy within the energy window. From the LEME configurations obtained using Basin Hopping Monte Carlo (BHMC) simulations, unique configurations are identified

by converting the chemical environment into graph representations using SurfGraph code developed by Deshpande et al.[51] The most energetically favourable structure (lowest Gibbs free energy) is shown by the red and black balls in Fig. 3(a-i) and the small variations are shown using the "clouds" of pink and grey balls (representing the oxygen and carbon atoms respectively).

As proposed by the experiments, the step edge is totally covered by on-top CO molecules.[24,26,32] CO adsorption results from the competition between stabilizing CO-surface interactions and destabilizing CO-CO lateral interactions that increase with CO coverage. Hence, the CO equilibrium coverage depends on the strength of the molecule-surface interaction and on the CO chemical potential (governed by T and P). Step sites correspond to a lower Pt coordination and hence a stronger CO-Pt interaction than the (111) terraces (see SI section 4). At the step, a coverage of 1 CO per Pt can be reached, but CO molecules present a different angular orientation to limit the CO-CO interactions. Such CO orientation leads to tilt angles from -25° to 46°, where negative angles represent tilt towards the upper terrace and positive angles representing tilt towards the lower terrace. Different tilt motifs are seen along the step edge with x2, x3, or x6 periodicities providing quasi-degenerate energies. At a chemical potential of -15.29 eV (corresponding to T=300K and P=1 atm), the most favorable coverage of CO is found to be 0.6 ML (as seen from Fig. 2(a)), with 54 structures in the LEME with this coverage. Fig. 3(b-e) represent the four CO arrangement patterns observed at this coverage (in decreasing stability order). In these structures, we find that CO molecules on the terrace arrange in distorted hexagonal patterns, the denser atomic directions being tilted ~25-36° with respect to the Pt step edge. These arrangements are limited by the short width of the terraces, but mimic the Moiré-like patterns seen on Pt(111). CO on the step Pt atoms interestingly arranges in a manner such that the quasi-hexagonal pattern on the lower terrace can be maintained. In a way the modulation of CO tilt angle along the step initiates the organisation of molecules on the lower terrace. Descending from the step to the lower terrace, the highly coordinated Pt atoms at the bottom of the step are not populated.

The lack of CO at the bottom of the step is also observed at other coverages throughout the LEME structures for Pt(553) and can be attributed to reducing the repulsion between the on-top step CO and the CO on the lower terrace. In contrast, the Pt row beyond the step edge on the upper terrace shows a high occupation of CO (0.5 - 0.83 ML). The coverage of 1 ML at the step edge implies a smaller coverage on the terrace of 0.5ML. The C-C distance at the densely populated step is between 2.8 and 3.0 Å (compared to 2.818 Å for the Pt-Pt distance), whereas the first C-C neighbor distance on the terrace varies between 3.2 and 3.4 Å, underlining the lower CO density on the terrace coming from a weaker adsorbate-surface interaction.

Three structures in the LEME are found at θ =0.56 which are shown in 3(a). At this low coverage, we don't see any systematic arrangement of CO on the terrace, but the step edge still has a 1 ML CO coverage. At θ =0.63, we see 3 different patterns (33 structures) of CO arrangement on Pt(553) shown in Fig.3(f-h) with increasing adsorption free energy order. All the structures at this coverage have a 6x1 periodicity with a tilt angle of -17° to 44° along the fully populated step edge. The CO coverage on the terrace is 0.54 (13 CO atoms on 24 Pt atoms). The CO arrangement on the terrace is less ordered compared to the arrangement found at θ = 0.6, making the quasi-hexagonal pattern less visible. At θ =0.65, we observe only a 4x1 unit cell periodicity along the step edge and 4 structures manifest in the LEME structures (Fig.2(i)). Similar to the structures found at θ =0.6, we find that CO molecules on the terrace arrange in distorted hexagonal patterns with the denser atomic directions being tilted ~55° with respect to the Pt step edge. A higher mobility of CO molecules is observed near the upper terrace, while the CO positions near the lower terrace and step edge remain approximately constant among the 4 structures. The C-C distance on the step with all CO molecules on the top site is between 2.8-3.0 Å and the first C-C neighbor distance on the terrace varies between 3.0-3.2 Å. At θ =0.67, we find one structures in the LEME with a 6x1 periodicity and CO arranging along parallel lines that are angled 55° (anti-clock wise) with respect to the step edge (see SI Fig. S5).

Overall, for Pt(553), the low energy metastable ensemble of structures has a coverage between 0.56 and 0.65. The short terrace length in combination with the (111)-type step only allows clear quasi-hexagonal arrangements of CO. The low coordination Pt atoms at the step site and the possibility of varying tilt angles of CO around the step edge enables a higher local coverage with CO adsorbing on the top site. On the terrace, C-C first neighbor distance decreases as the coverage increases to incorporate more CO on the surface. Comparing the site distribution on the terrace, we see that the majority of the structures have a higher top site coverage followed by hollow site occupation and the least occupied sites are the bridge sites.

2.2 Pt(557)

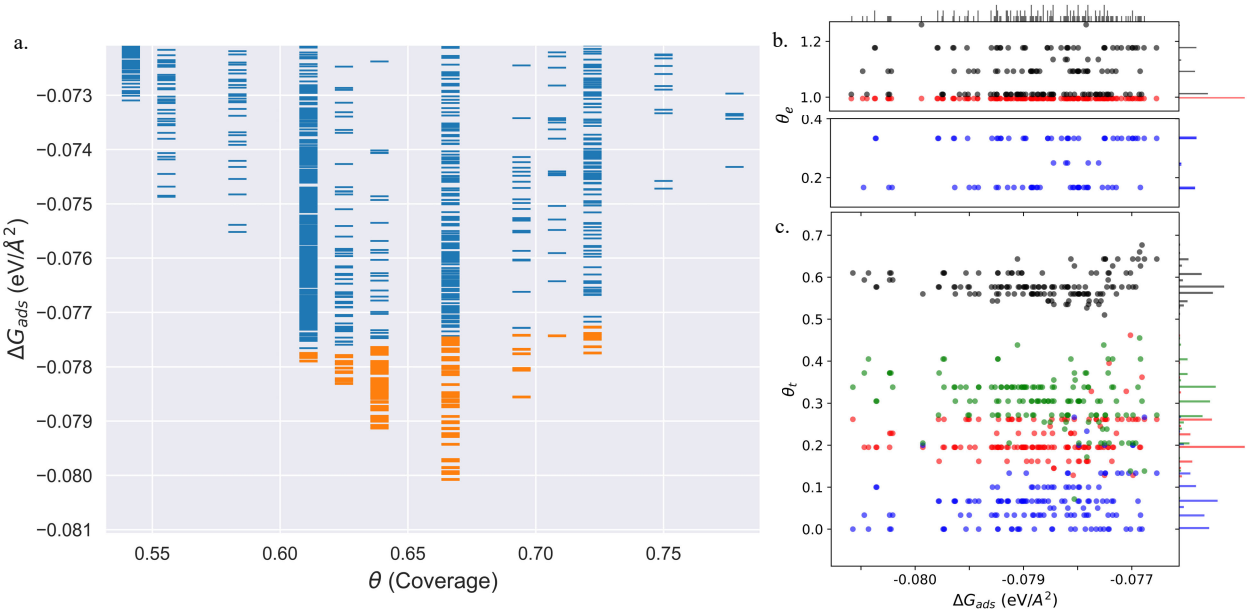

Figure 4: (a) Adsorption Free energy per unit area (ΔG_{ads}) plotted against CO coverage (θ) on Pt(557). Yellow markers represents the structures defining the LEME.(b) and (c) represent the coverage of CO on the Pt step-edge and terrace as a function of the ΔG_{ads} respectively. ● represents top site, ● represents bridge site, ● represents hollow site and ● represents the total coverage. The points in (b) and (c) have been moved in a similar fashion as Fig. 2 to distinguish the points better.

Pt(557) can be represented as Pt[6(111) × (100)] in step notation since it is formed by a 6 atom wide Pt(111) terrace followed by a mono-atomic 100-type step as shown in Fig.

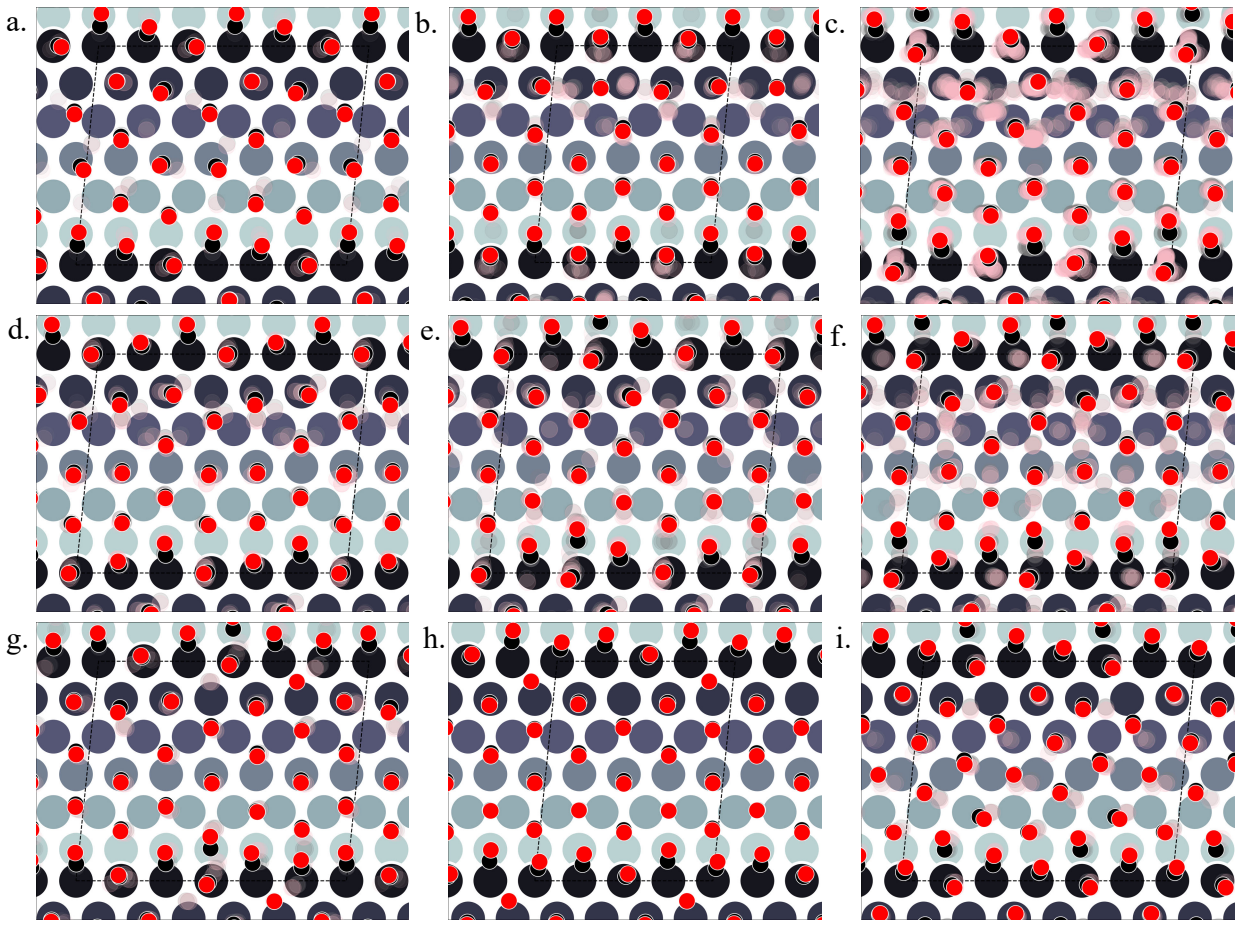

Figure 5: Various structures of CO orientations patterns observed in the LEME for Pt(557). (a) represents structures with θ = 0.61; (b) with θ = 0.625; (c) with θ = 0.64; (d-f) with θ = 0.66, (g) with θ = 0.69, (h) with θ = 0.71, and (i) with θ = 0.72. The Pt atoms are shown using a colormap (color-bar representing z-position of the Pt atom). For a given pattern, the lowest energy orientation of CO is shown using the solid black and red balls representing the positions of C and O respectively and the ensemble of structures are represented by the "cloud" of pink and grey balls.

1(c) and (d). We use 3x1, 4x1, and 6x1 unit cells to explore the CO organization on the surface. The low energy CO configurations on Pt(557) at RT and 1 atm CO pressure found by our HDNNP and basin hopping approach correspond to coverages between 0.61 ML and 0.72 ML with 142 structures in the LEME (Fig.4(a)). Similar to the Pt(553), the step site is completely occupied by on-top CO molecules. However, the more open character of the (100) steps permits to have in addition CO molecules bridging between a step edge atom and one Pt immediately below in the lower terrace. The step edge atom can hence be bound to two CO molecules, one top and one bridge. In that case (as seen in figure 5(c,e-g and i), the top

molecule is not leaning towards the lower terrace, but towards the upper terrace. With that mechanism, the coverage at the step can reach up to 1.25 ML (the bridging CO molecule is shared between the two Pt atoms (Fig. 4(b))). The uneven tilt of the CO molecules at the step edge initiates the organisation on the terrace, with quasi-hexagonal ordering throughout the LEME and helps incorporate higher coverage on the square step. The tilt angles range between -20° and 50° with x2 and x3 periodic motifs that provide quasi-degenerate energies. For the structures in the LEME, on terrace, the coverage ranges from 0.50 to 0.67 ML , with on average, hollow sites dominating with a coverage of 0.3 ML, top sites with 0.22 ML and bridge sites at 0.06 ML (Fig. 4(c)). Hence, on average, on the terrace, multiply bounded CO on the terrace is in average almost twice that of the top site. This strongly contrasts with the previous case of Pt(553) where on the on-top CO was dominating on the terrace, indicating that the type of step has a strong influence on the configuration of CO molecules.

At 300K and 1 atm condition, the most stable structure is found at θ =0.67. At this coverage, we find three types of CO arrangements as shown in Fig. 5(d),(e) and (f) (in the stability order). For the most stable structure at θ =0.67, CO arranges along parallel lines that are tilted ~30° with respect to the Pt step edge (Fig. 5(d) - arrangement shown using black and red balls). Such a positioning of CO molecules on the terrace, which is accompanied by the CO molecules creating a x3 motif on the step with varying tilts towards the lower terrace, helps create a quasi-hexagonal pattern. Change of CO positions at the lower terrace (mainly between hollow and bridge site) results in quasi-degenerate LEME structures that have been represented by the pink and gray "clouds" in Fig. 5. At the same coverage, we find another orientation of CO at the step edge (with a x2 motif) with alternating CO molecules tilting towards and away from the lower terrace (Fig. 5(e)). At this coverage, the C-C distance (first neighbor) varies between 2.7-3.18 Å on the terrace and 2.8-3.18 Å on the step edge.

Within the LEME, lower coverage structures are found with θ =0.61 (4 structures), θ =0.625 (12 structures), and θ =0.64 (59 structures). At higher coverages, LEME includes

structures with θ =0.69 (6 structures), θ =0.71 (1 structure), θ =0.72 (8 structure). At these coverages, the quasi-hexagonal pattern is maintained on the terrace and the step coverage remains 1 ML as seen in Fig. 5. The CO quasi-hexagonal lattice rotation with respect to the step edge, is coverage dependent. At θ =0.61, CO arranges along parallel lines that are tilted ~23.5°. At θ =0.625 and θ =0.64, the angle increases to 30° and at θ =0.66 the tilt angle further increases to ~40°. Further increase in coverage leads to reduction in the tilt angle to 30-35° at θ =0.69 and θ =0.71 and to ~20° at θ =0.72. The different rotation angles of the CO lattice allows maintaining approximately similar C-C first neighbor distances on the terrace (~3.15-3.22) while allowing more CO to be incorporated on the surface. Though out the LEME ensemble, the step manifests a x2 or x3 repeating motif. Except at θ =0.61 and θ =0.71, all the other structures in the LEME show additional CO molecules bridging between the step edge and lower terrace allows for incorporating more CO on the surface. This increasing the step edge coverage to 1.17 ML.

Overall, for Pt(557), the low energy metastable ensemble of structures has a coverage between 0.61 and 0.72, slightly higher than the case of Pt(553). The formation of a more ordered hexagonal pattern for the CO adsorbates on the Pt substrate can be attributed to the longer terrace length and the square Pt(100) step. One striking difference concerns the binding sites of CO on the terrace, with the dominant multiply bonded CO on the (557) surface, while top sites were twice more numerous on the (553) termination. The more open Pt(100) step allows CO bridging between the terrace and the step edge which in turn allows the hexagonal pattern of CO lattice to continue across the stepped surface. These three factors have a significant impact on the CO arrangement on the surface.

2.3 Pt(643)

The Pt(643) surface consists of Pt(111) terraces separating Pt(100) steps that are broken by Pt(110) kink sites. The kink shows a convex site on a 6-coordinated Pt atom, next to a concave site on a 8-coordinated Pt atom (Fig. 1(e,f)). Basin hopping simulations using

the neural network potential were run on a (2x1) unit cell (creating a 6 Pt atom step edge with the kink site) which showed a CO coverage from 0.5 to 0.65 ML (Fig. 6(a)) in the low energy minima ensemble of structures (20 structures) at 300 K and 1 atm conditions, the most stable structure having a coverage of 0.6 ML. The coverage of CO on the Pt step edge (θ_e), is shown in Fig. 6(b). In the ensemble, 4 structures show θ_e =0.83 ML and 16 structures show θ_e =1.0 ML. Two structures (with θ_e =1 ML and θ =0.7 ML) have CO on the bridge site at the concave site of the kink, which are shown using blue points on Fig. 6(b). For all the other structures, CO occupies the top site on the step edge and kink atoms. Compared to Pt(553) and Pt(557), Pt(643) has a smaller terrace length which does not allow a similar rotated hexagonal pattern arrangement of CO. On the contrary, the short terrace combined with the the kink site and the square step edge forces the CO organization parallel to the dense Pt atoms arrangement throughout the LEME structures. The short terrace also limits the number of structures in the LEME, the adsorbate layer being less fluxional.

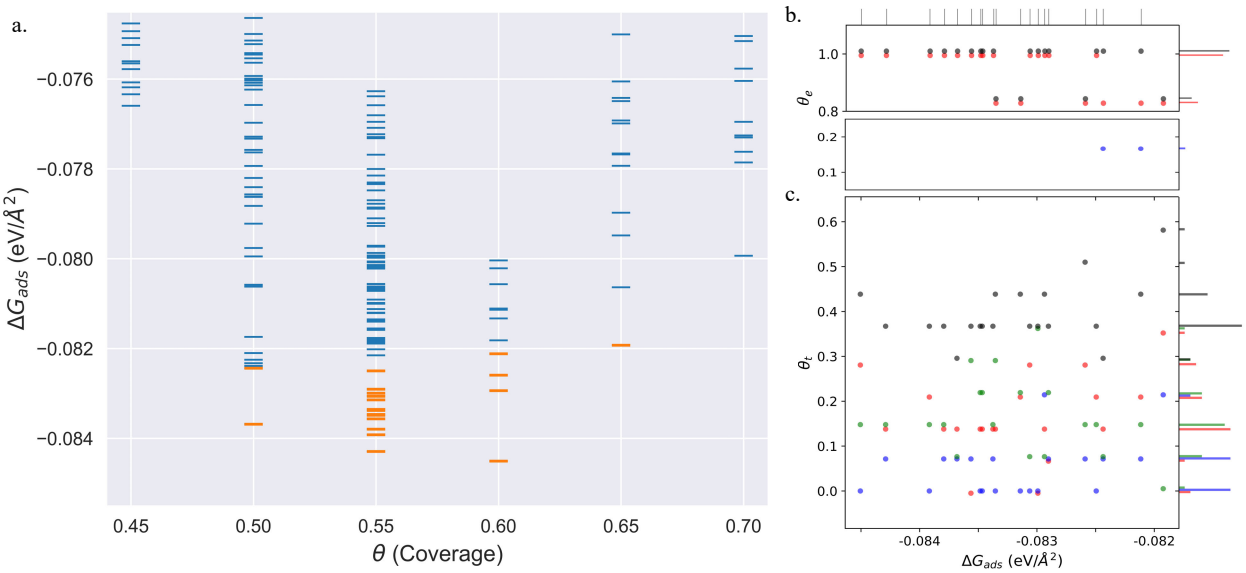

Figure 6: (a) Adsorption Free energy per unit area (ΔG_{ads}) plotted against CO coverage (θ) on Pt(643). Yellow markers represents the structures defining the LEME.(b) and (c) represent the coverage of CO on the Pt step-edge and terrace as a function of the ΔG_{ads} respectively. ● represents top site, ● represents bridge site, ● represents hollow site and ● represents the total coverage. The points in (b) and (c) have been moved in a similar fashion as Fig. 2 to distinguish the points better.

At θ =0.5, 2 structures exist in the LEME (Fig. 7(a)). At this coverage, the step sites are

fully covered with on-top CO and on the terrace top to bridge ratio is 1:1. The CO assembly at this coverage is less ordered, which results in more distributed positions. At θ =0.55, 13 structures ((Fig. 7(b))) are observed in the LEME which have all except two structures with low coordination step Pt atoms have a θ_e =1 ML and the remaining two have a θ_e =0.83 ML. At this coverage, on average over the LEME structures, the top to hollow site occupation ratio on the terrace is approximately 1:1 while bridge site occupation is negligible. The tilt of CO molecules at the kink atom can be large ($\sim 40^\circ$). On the terrace, at θ =0.55, the parallel CO arrangement is broken near the kink site.

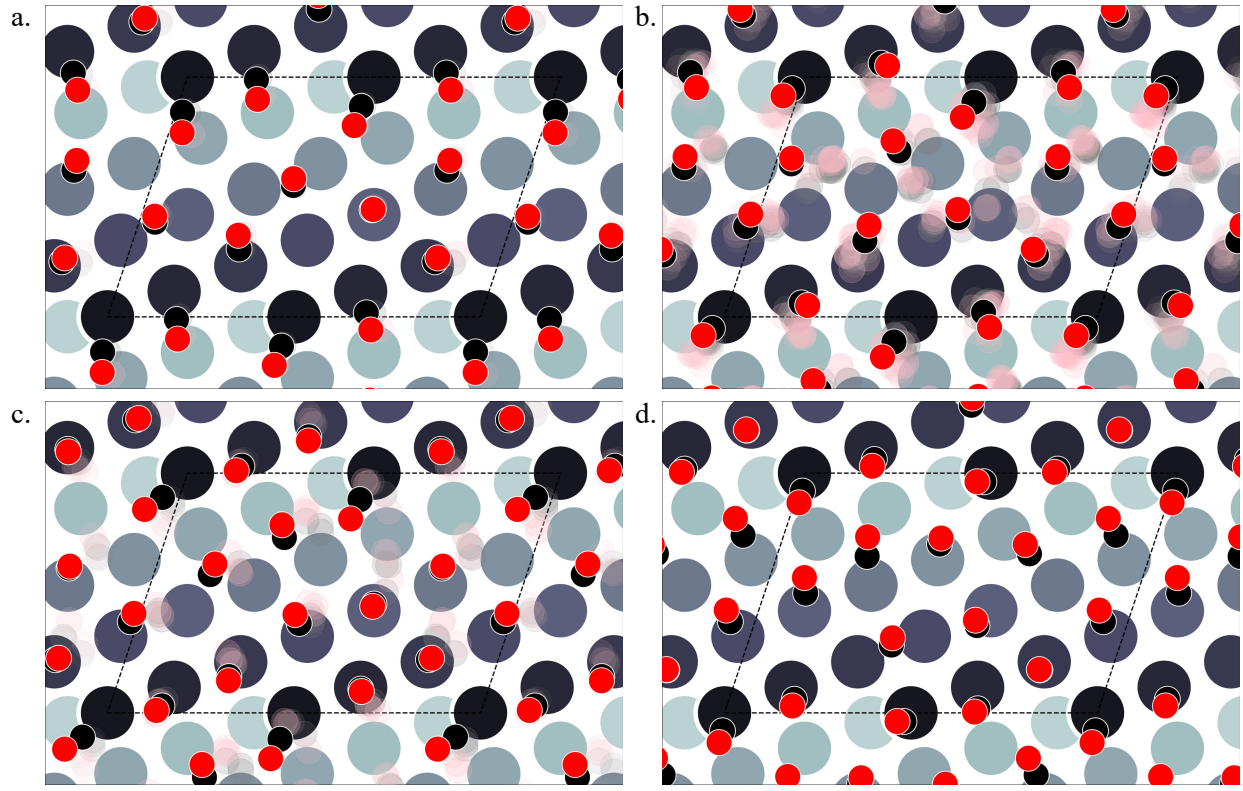

Figure 7: Various structures of CO orientations patterns observed in the LEME for Pt(643). (a) represent structures with θ = 0.5; (b) with θ = 0.55; (c) with θ = 0.6 and (d) with θ = 0.65. The Pt atoms are shown using a colormap (color-bar representing z-position of the Pt atom). For a given pattern, the lowest energy orientation of CO is shown using the solid black and red balls representing the positions of C and O respectively and the ensemble of structures are represented by the "cloud" of pink and grey balls.

The most stable structure on Pt(643) is found at a θ =0.6 and is shown in Fig. 7(c). Similar to the structures at θ =0.55, CO align along lines that are parallel to the step edge

but the symmetry is maintained throughout. In the ensemble at this coverage, θ_e varies from 0.83-1 ML and all CO adsorbed at the step occupy the top site. CO molecules on the terrace occupy the top (on average 0.23 ML) and hollow sites(on average 0.125 ML) with only minor (or no) occupation of bridge sites. The short terrace and parallel arrangement of CO with respect to the substrate Pt atoms possibly does not allow the bridge site occupation. At θ =0.65, we find only 1 structures in the LEME as shown in 7(d) where we observe similar arrangement of CO as for θ =0.55, where the CO alignment pattern is broken near the kink Pt atom site. At this coverage, once again top sites dominate the occupation on the terrace with 0.36 ML.

Overall, on Pt(643), we see a combined effect of a kink site, square step and a small terrace length which leads to an arrangement of CO that aligns parallel to the step edge. On average across the LEME structures we find an equal occupation of top and hollow sites while bridge occupation is limited. Such a behaviour is unique compared to Pt(553) and Pt(557) where we saw a development of hexagonal patterns of CO arrangement. Understanding the CO organization on such a surface with kinks and step can be important since the low coordination kink site appearing on this surface can show specific catalytic activity and also can be the starting point of restructuring event under CO pressure.

3 Conclusion

The organization of CO adsorbates on different surfaces including steps and kinks and presenting (111) terraces was modelled under an ambient pressure of CO at room temperature, by combining a neural network potential, trained using first principle structures, including energies and forces, and a basin hopping approach to efficiently explore the various configurations of the CO adsorbates, describing an extensive number of structures (~4500). The main conclusions are summarized below. In the considered conditions, the step edge (or kink) is totally occupied by on-top CO molecules, while terraces show a partial occupation

close to 0.5 ML. One recurring feature is that the surface (Pt(553), Pt(557) or Pt(643)) does not show a single most stable CO adsorption structure at the considered CO chemical potential, but that a large number of adsorbate configurations on the terrace are close in energy. By considering a threshold of 1 kT per CO adsorbate, we defined the LEME, ensemble of structures thermally accessible, which contain 97, 142 and 20 distinct structures for the considered Pt(553), Pt(557) and Pt(643) unit cells respectively. These structures show imperfect quasi-hexagonal ordering on the terraces, while the arrangement along the step edge is more ordered, including different tilts with respect to the terrace normal to decrease CO-CO interactions. The large number of competing structures should result in a mixture of very small domains of different configurations, and hence an absence of long range order, as seen in the experiments. Some common results arise from this study. The first one concerns the distribution between top and multiply bonded CO on the (111) terraces. Stable adsorption configurations on the Pt(553) surface present more top site CO than multiply bonded ones on the (111) terrace, resulting in average in two top site CO for one multiply bonded CO. The situation is completely modified on the (111) terraces of the (557) surface, where in average two multiply bonded CO are seen for one top CO. On the kinked Pt(643) surface, the top CO molecules again dominate on the surface. These results should be compared with the extended Pt(111) surface where in the same conditions an equal number of top and multiply bonded CO molecules are found. The three considered surfaces show different structures of the step edge: a (111) step for Pt(533), a (100) step for Pt(557) and a kink site with a short terrace for Pt(643). Since the binding energy of top CO is very close to that of multiply bonded CO on the (111) terrace, the structure of the step plays a key role in initiating the arrangement of CO on the lower terrace, since the CO at the step with their different amount of tilt towards the terrace act as a boundary condition to organize the adsorbates on the terrace. The (111) steps favor the construction of quasi-hexagonal layers where top site CO dominates, presenting alignments of CO at various possible angle with respect to the step edge, while in contrast the (100) steps pin configurations with a large

fraction of multiply bonded sites.

Our calculated results agree well with the experimental data from Farias at al. in electrochemical conditions where Pt(322) and Pt(311) surfaces, that present a (100) step, show a large amount of bridge site CO on their terraces, while Pt(332) and Pt(331) surfaces, with a (111) step, show a very large majority of top site CO.[32] They also agree with the UHV experiments of Tränkenschuh et al. in the case of Pt(553)).[24] The kink surface (Pt(643)) shows a different type of arrangement where CO aligns parallel to the step edge. This demonstrates that the atomic arrangement at the steps controls the structure of the CO ad-layers at least in a zone close to the step edge.

Understanding CO adsorption at stepped surfaces is a prerequisite to study their catalytic reactivity in reactions involving CO. It is also of key importance as the initial structure leading to surface restructuring upon CO adsorption at ambient pressure. Indeed, extended Pt step edges are known to undergo reconstruction driven by CO adsorption at high coverage. Our study opens the way to realistic modelling of these restructuring events.

4 Methods

4.1 First Principle Calculation Details

Calculations were performed using the Vienna Ab-initio Simulation Package[52–55] using the general gradient approximation (GGA) Perdew-Burke-Erzenhof (PBE) functional.[56] Core electrons were described using the projector augmented wave potentials.[57,58] A k-spacing of 0.25 is used for all the calculations and the generated k-point grid is centered at the Γ point. Periodic slabs of Pt surface with CO are separated by 12 Å vacuum in the z direction. A fermi smearing width of 0.2 eV was applied using the Methfessel-Paxton method (order 2). A cutoff energy of 400 eV is used. The known issue of overbinding of CO on Pt surfaces ("Pt(111)/CO Puzzle") has been corrected using the CO bond distance-based correction developed by us.[20] The generalized correction is given as $\Delta = 4.77 * d_{CO} - 5.37$, where Δ is

the correction applied in (eV) and d_{CO} is the bond length of adsorbed CO in (Å).

4.2 Training a High Dimensional Neural Network Potential

We exploit the use of HDNNP to define the atomic potential for Pt/CO system to reduce the computational cost and explore the potential energy surface (PES) efficiently. The assumption in developing the HDNNP is that there exists a unique functional relation between the atomic coordinates and the potential energy. Using HDNNP, the total energy of the system is defined as a the sum of individual atomic contributions, $E_s = \sum E_i$, where the atomic energy E_i is found by training atomic Neural Networks using the structural and chemical environments ($E_s = \sum NN(X_i^{env})$). These environments are defined using various feature transformations (descriptors) that convert Cartesian coordinates, which are not invariant with respect to translation and rotation of the system to invariant representations implemented using Atom-centered Symmetry Functions (ACSF)[59], smooth overlap of atomic positions (SOAP)[60], Many-body Tensor Representation (MBTR)[61], etc.

In this work, we use the high-dimensional neural network potential where the R_i^{α} (Cartesian coordinates α of atom i) are transformed into a set of symmetry function values G_i^{μ} for each atom i.[62]. The developed NN utilises 2 hidden layers with 30 nodes each and a hyperbolic tangent activation function. A total of 46 symmetry functions were used for each element - Pt, C, and O. We use the weighted atom-centered symmetry function (wACSF) proposed by Gastegger et. al which can be repressed as:[63]

$$G_i^2 = \sum_{j \neq i} Z_j \mathrm{e}^{-\eta (r_{ij} - r_s)^2} f_c(r_{ij}) \tag{1}$$

$$G_i^3 = 2^{1-\zeta} \sum_{\substack{j,k \neq i \\ j<k}} Z_j Z_k \left(1 + \lambda \cos\theta_{ijk}\right)^{\zeta} \mathrm{e}^{-\eta \left[(r_{ij}-r_s)^2 + (r_{ik}-r_s)^2 + (r_{jk}-r_s)^2\right]} f_c(r_{ij})\, f_c(r_{ik})\, f_c(r_{jk}) \tag{2}$$

$$f_c(r_{ij}) = ((15 - 6r_{ij})r_{ij} - 10)r_{ij}^3 + 1 \tag{3}$$

where, G_i^2 represents the radial symmetry function and G_i^3 represents the angular symmetry

function. f_c represents a polynomial cutoff function. $r_{ij} = |\mathbf{r}_i - \mathbf{r}_j|$ represents the interatomic distance between atom i and j and $\theta_{ijk} = (\mathbf{r}_{ij} \cdot \mathbf{r}_{ik})/(|\mathbf{r}_{ij}||\mathbf{r}_{ik}|)$ represents the angle spanned by the atoms i, j, and k. $Z_{i/j/k}$ represents the atomic numbers which are used as weights for the symmetry functions. The parameters η and r_s have been determined using the automatic selection algorithm developed by Imbalzano et. al based on equally dividing the cutoff radius (r_c = 6 Å) in n intervals which is chosen here to be 5. Two sets of radial symmetry functions (G^2) are used: (i) the first group centered on the reference atom ($r_s = 0$) with $\eta = 0.0278, 0.0529, 0.1007, 0.1916, 0.3648, 0.6944$ (6 symmetry functions) and (ii) second group is centered along the path between the central atom and its neighbour with r_s =1.5, 2.1213, 3, 4 and η = 2.5904, 1.2952, 0.6476, 0.3238 respectively (4 symmetry functions). 36 angular symmetry functions (G^3) have been defined with r_s = 0; η = 0.0278, 0.0529, 0.1007, 0.1916, 0.3648, 0.6944; λ = -1,1 and ζ = 1, 4, 16. This creates atomic NN architectures that can be represented as 46-30-30-1.

The reference database is built iteratively. Starting from an initial reference data set (consisting of Pt(111) surface with different unit cell sizes and CO coverages), a first preliminary HDNNP is obtained. This HDNNP is used with BHMC simulations to generate more relevant data, which is used to validate the potential to check for extrapolations and missing Potential Energy Surface (PES) data. If the accuracy of the developed potential is insufficient, problematic structures are identified and added to the training set until a converged potential is obtained. Fig. S3 in the SI shows a flowchart explaining this iterative process of HDNNP development. In every iteration of the training, 10% of the total reference data generated is used as a validation fraction and over fitting is avoided by using the early stop algorithm. The final reference database consisted of 4289 structures. We used the n2p2 package for training.[64] This package provides an efficient approach for optimizing the weight parameters of the neural network via multi-stream Kalman filtering, using potential energies and atomic forces as reference data. A loss function for the training is defined as the sum of energy and force RMSE (root mean square error), i.e., force coefficient $\gamma = 1$. For re-usability

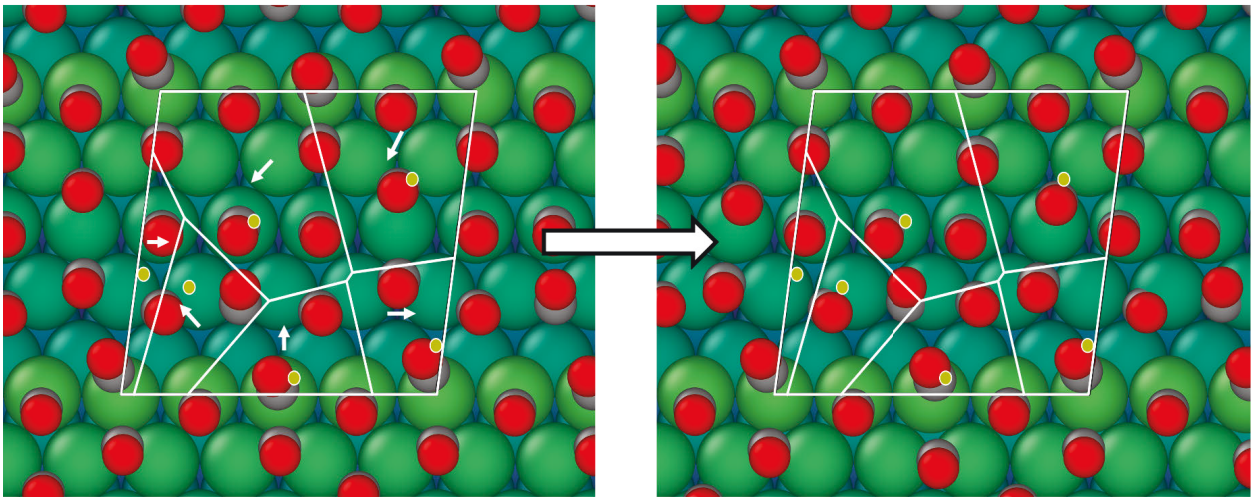

Figure 8: Clustering mutation algorithm implemented with the Basin Hopping algorithm. The dark gray balls represent carbon atoms and red balls represent oxygen atoms. The light gray balls are the substrate platinum atoms. The blue lines define the Voronoi tessellation and the yellow dots represent the centers for the Voronoi clusters. Atoms within one cluster are moved randomly in the same direction as seen in the model implementation.

of the developed potential, we include the output weight parameter and other files in the Supporting Information. The "input.nn" file includes all variables needed to reproduce the NN as well, including symmetry functions, cutoff radius, and hidden layers and nodes and the "weights.*.data" contains the weights of the atomic NNs.

4.3 Basin Hopping Monte Carlo (BHMC) Simulation

Basin Hopping method is a frequently used global optimization method for finding low energy structures. For our purposes, we use the method to generate new structures by taking advantage of the efficient HDNNP to quickly sample the configuration space that can be then recalculated by DFT to add to the reference database. This algorithm take advantage of basin hopping method and Monte Carlo method with local minimization to convert the potential energy surface (PES) from a curved surface to stepped shape basins.[65]. The exploration of these basins is achieved by Monte Carlo sampling through atomic displacements and the Metropolis criterion. The free energy is calculated by subtracting the reference chemical potential (which is a function of temperature and pressure) of the adsorbate from the energy

of the system as shown by the following equations:

$$\Delta G = E(nCO + slab) - E(slab) - n_{CO} \times \mu_{CO} \tag{4}$$

where $E(nCO + slab)$ is the electronic energy of the optimized structure, $E(slab)$ is the energy of the optimized bare Pt slab and μ_{CO} is the chemical potential of CO in the gas phase. Translational and rotational terms are taken into account to calculate the CO gas phase chemical potential, but vibrational terms are not included, since they are neglected in the CO adsorbed state as well.

The Metropolis criterion implies that a MC move is always accepted if the free energy of the new structure ΔG_{new} is lower than the previous structure, ΔG_{old}, otherwise it is accepted with a probability $\exp[(\Delta G_{old} - \Delta G_{new})/k_B T_{MC}]$, which is determined by a random number drawn from the interval [0,1]. Here, the "temperature" for BH simulation (T_{MC}) is an adjustable parameter. Based on the acceptance and rejection of the structures while running the BH simulation, this parameter can be adjusted. A flow chart explaining the BHMC algorithm used in this work has been included in the SI (Fig. S1 and S2). BHMC algorithm differs from the standard MC algorithm in one step namely the local optimization that is performed at each point of the PES and since the BHMC exploration is performed by hopping among different basins, a larger atomic displacement (Δr_i) can be used compared to standard MC. Both these features of BHMC simulations help increase the success rate in obtaining the global minima. Most BHMC implementations utilize random atomic displacements.[66–68] For high coverage of CO on Pt surfaces, random perturbation of adsorbate atoms leads to a low acceptance ratio (~20%) since the motion of one CO molecule on the surface is only allowed if the neighboring adsorbed molecules move in a concerted manner. As a result, we introduced a new kind of move, "Clustering mutation algorithm", where we cluster a few adsorbed molecules randomly and move all in the same random motion together. This was done by dividing the surface into Voronoi tessellations using random center points within

the unit cell. Such a move in conjunction with random atomic displacements significantly improved the exploration of the potential energy surface and increased the acceptance ratio (~50%). The algorithm is explained in more detail in the SI.

HDNNP is efficiently used with BHMC to explore the PES and find the low energy minima ensemble of structures. Since the HDNNP is not fully accurate, the ordering of structures based on energies is not the same as predicted by the HDDNP when compared with DFT calculations. As a result, we recalculate with DFT all structures that have free energy $G <= G_{min} + 0.05eV/\text{Å}^2$ which is a significantly higher error margin than the error expected from the HDNNP. This ensures that we have recalculated all the low energy minima ensemble of structures, which is then used to report the relative adsorption free energies and the minima structures. The (i) BHMC code, (ii) training, validation and test dataset and (iii) HDNNP files are made available on Github.[69]

5 Acknowledgment

This work was funded by NSF, Grant No. 1800601. This work used computational and storage services associated with the Hoffman2 Shared Cluster provided by the UCLA Institute for Digital Research and Education's Research Technology Group. The authors want to thank XSEDE (TG-CHE170060) SDSC's Expanse Supercomputer and Bridges PSC for the compute time.

References

(1) Somorjai, G. A.; Blakely, D. Mechanism of catalysis of hydrocarbon reactions by platinum surfaces. *Nature* **1975**, *258*, 580–583.

(2) Somorjai, G. A. Surface science and catalysis. *Science* **1985**, *227*, 902–908.

(3) Sun, S.-G.; Chen, A.-C.; Huang, T.-S.; Li, J.-B.; Tian, Z.-W. Electrocatalytic properties

of Pt(111), Pt(332), Pt(331) and Pt(110) single crystal electrodes towards ethylene glycol oxidation in sulphuric acid solutions. *Journal of Electroanalytical Chemistry* **1992**, *340*, 213–226.

(4) Baltruschat, H.; Bußar, R.; Ernst, S.; Hernandez, F. *In-Situ Spectroscopic Studies of Adsorption at the Electrode and Electrocatalysis*; Elsevier, 2007; pp 471–537.

(5) Tian, N.; Zhou, Z.-Y.; Sun, S.-G. Platinum metal catalysts of high-index surfaces: from single-crystal planes to electrochemically shape-controlled nanoparticles. *The Journal of Physical Chemistry C* **2008**, *112*, 19801–19817.

(6) Yates, J. T. Surface chemistry at metallic defect sites. *J. Vac. Sci. Technol. A* **1995**, *13*.

(7) Taylor, H. S. A theory of the catalytic surface. *Proc. R. Soc. Lond. A* **1925**, *108*.

(8) Hammer, B.; Nielsen, O. H.; Nørskov, J. K. Structure sensitivity in adsorption: CO interaction with stepped and reconstructed Pt surfaces. *Catal. Lett.* **1997**, *46*.

(9) Somorjai, G. A. *Introduction to Surface Chemistry and Catalysis*; 1994.

(10) Zambelli, T.; Wintterlin, J.; Trost, J.; Ertl, G. Identification of the 'active sites' of a surface-catalyzed reaction. *Science* **1996**, *273*.

(11) Dahl, S. Role of steps in N_2 activation on Ru(0001). *Phys. Rev. Lett.* **1999**, *83*.

(12) Geerlings, J. J. C. Fischer–Tropsch technology—from active site to commercial process. *Appl. Catal. A* **1999**, *186*.

(13) Vang, R. T. Controlling the catalytic bond-breaking selectivity of Ni surfaces by step blocking. *Nature Mater.* **2005**, *4*.

(14) Somorjai, G. Surface reconstruction and catalysis. *Annual Review of Physical Chemistry* **1994**, *45*, 721–751.

(15) Tao, F.; Dag, S.; Wang, L.-W.; Liu, Z.; Butcher, D. R.; Bluhm, H.; Salmeron, M.; Somorjai, G. A. Break-up of stepped platinum catalyst surfaces by high CO coverage. *Science* **2010**, *327*, 850–853.

(16) Tao, F.; Crozier, P. A. Atomic-scale observations of catalyst structures under reaction conditions and during catalysis. *Chemical reviews* **2016**, *116*, 3487–3539.

(17) Nguyen, L.; Cheng, F.; Zhang, S.; Tao, F. Visualization of Surfaces of Pt and Ni Model Catalysts in Reactive Environments Using Ambient Pressure High Temperature Scanning Tunneling Microscopy and Understanding the Restructurings of Surfaces of Model Metal Catalysts under Reaction Conditions at Near Ambient Pressure. *The Journal of Physical Chemistry C* **2013**, *117*, 971–977.

(18) Avanesian, T.; Dai, S.; Kale, M. J.; Graham, G. W.; Pan, X.; Christopher, P. Quantitative and atomic-scale view of CO-induced Pt nanoparticle surface reconstruction at saturation coverage via DFT calculations coupled with in situ TEM and IR. *Journal of the American Chemical Society* **2017**, *139*, 4551–4558.

(19) Zhao, X.; Perry, S. S.; Horvath, J. D.; Gellman, A. J. Adsorbate induced kink formation in straight step edges on Cu(533) and Cu(221). *Surface science* **2004**, *563*, 217–224.

(20) Sumaria, V.; Nguyen, L.; Tao, F. F.; Sautet, P. Optimal Packing of CO at a High Coverage on Pt(100) and Pt(111) Surfaces. *ACS Catalysis* **2020**, *10*, 9533–9544.

(21) Longwitz, S. R.; Schnadt, J.; Vestergaard, E. K.; Vang, R. T.; Lægsgaard, E.; Stensgaard, I.; Brune, H.; Besenbacher, F. High-coverage structures of carbon monoxide adsorbed on Pt(111) studied by high-pressure scanning tunneling microscopy. *The Journal of Physical Chemistry B* **2004**, *108*, 14497–14502.

(22) Vestergaard, E. K.; Thostrup, P.; An, T.; Lægsgaard, E.; Stensgaard, I.; Hammer, B.; Besenbacher, F. Comment on "High pressure adsorbate structures studied by scanning

tunneling microscopy: CO on Pt(111) in equilibrium with the gas phase". *Physical review letters* **2002**, *88*, 259601.

(23) Jensen, J. A.; Rider, K. B.; Salmeron, M.; Somorjai, G. A. High pressure adsorbate structures studied by scanning tunneling microscopy: CO on Pt(111) in equilibrium with the gas phase. *Physical review letters* **1998**, *80*, 1228.

(24) Tränkenschuh, B.; Fritsche, N.; Fuhrmann, T.; Papp, C.; Zhu, J.; Denecke, R.; Steinrück, H.-P. A site-selective in situ study of CO adsorption and desorption on Pt(355). *The Journal of chemical physics* **2006**, *124*, 074712.

(25) Henderson, M.; Szabo, A.; Yates Jr, J. Direct observation of adsorbate dynamics from low-frequency vibration on a step defect—CO on Pt (112). *The Journal of chemical physics* **1989**, *91*, 7255–7264.

(26) Hopster, H.; Ibach, H. Adsorption of CO on Pt(111) and Pt 6 (111)×(111) studied by high resolution electron energy loss spectroscopy and thermal desorption spectroscopy. *Surface Science* **1978**, *77*, 109–117.

(27) Lang, J.; Masel, R. An XPS study of nitric oxide, carbon monoxide and oxygen adsorption on Pt(210). *Surface science* **1986**, *167*, 261–270.

(28) Gland, J. L.; McClellan, M. R.; McFeely, F. R. Carbon monoxide oxidation on the kinked Pt(321) surface. *The Journal of chemical physics* **1983**, *79*, 6349–6356.

(29) Luo, J.; Tobin, R.; Lambert, D. K.; Fisher, G. B.; DiMaggio, C. L. CO adsorption site occupation on Pt(335): a quantitative investigation using TPD and EELS. *Surface science* **1992**, *274*, 53–62.

(30) Baro, A.; Ibach, H. New study of CO adsorption at low temperature (90 K) on Pt(111) by EELS. *The Journal of chemical physics* **1979**, *71*, 4812–4816.

(31) Ibach, H.; Bruchmann, D. Surface Phonons on Stepped Pt(111) Surfaces. *Physical Review Letters* **1978**, *41*, 958.

(32) Farias, M. J.; Busó-Rogero, C.; Tanaka, A. A.; Herrero, E.; Feliu, J. M. Monitoring of CO Binding Sites on Stepped Pt Single Crystal Electrodes in Alkaline Solutions by in Situ FTIR Spectroscopy. *Langmuir* **2019**, *36*, 704–714.

(33) Wang, K.; Ming, F.; Huang, Q.; Zhang, X.; Xiao, X. Study of CO diffusion on stepped Pt (1 1 1) surface by scanning tunneling microscopy. *Surface science* **2010**, *604*, 322–326.

(34) Behler, J.; Parrinello, M. Generalized neural-network representation of high-dimensional potential-energy surfaces. *Physical review letters* **2007**, *98*, 146401.

(35) Boes, J. R.; Kitchin, J. R. Neural network predictions of oxygen interactions on a dynamic Pd surface. *Molecular Simulation* **2017**, *43*, 346–354.

(36) Zhu, L.; Zhang, Y.; Zhang, L.; Zhou, X.; Jiang, B. Unified and Transferable Description of Dynamics for H_2 Dissociative Adsorption on Multiple Copper Surfaces via Machine Learning. *Physical Chemistry Chemical Physics* **2020**,

(37) Gerrits, N.; Shakouri, K.; Behler, J.; Kroes, G.-J. Accurate probabilities for highly activated reaction of polyatomic molecules on surfaces using a high-dimensional neural network potential: CHD_3+ Cu(111). *The journal of physical chemistry letters* **2019**, *10*, 1763–1768.

(38) del Cueto, M.; Zhou, X.; Zhou, L.; Zhang, Y.; Jiang, B.; Guo, H. New Perspectives on CO_2-Pt (111) Interaction with a High-Dimensional Neural Network Potential Energy Surface. *The Journal of Physical Chemistry C* **2020**, *124*, 5174–5181.

(39) Kolb, B.; Luo, X.; Zhou, X.; Jiang, B.; Guo, H. High-dimensional atomistic neural

network potentials for molecule–surface interactions: HCl scattering from Au(111). *The journal of physical chemistry letters* **2017**, *8*, 666–672.

(40) Shakouri, K.; Behler, J.; Meyer, J.; Kroes, G.-J. Accurate neural network description of surface phonons in reactive gas–surface dynamics: N_2+ Ru(0001). *The journal of physical chemistry letters* **2017**, *8*, 2131–2136.

(41) Liu, Q.; Zhou, X.; Zhou, L.; Zhang, Y.; Luo, X.; Guo, H.; Jiang, B. Constructing high-dimensional neural network potential energy surfaces for gas–surface scattering and reactions. *The Journal of Physical Chemistry C* **2018**, *122*, 1761–1769.

(42) Zhang, Y.; Zhou, X.; Jiang, B. Bridging the gap between direct dynamics and globally accurate reactive potential energy surfaces using neural networks. *The Journal of Physical Chemistry Letters* **2019**, *10*, 1185–1191.

(43) Huang, M.; Zhou, X.; Zhang, Y.; Zhou, L.; Alducin, M.; Jiang, B.; Guo, H. Adiabatic and nonadiabatic energy dissipation during scattering of vibrationally excited CO from Au (111). *Physical Review B* **2019**, *100*, 201407.

(44) Wales, D. J.; Doye, J. P. K. Global Optimization by Basin-Hopping and the Lowest Energy Structures of Lennard-Jones Clusters Containing up to 110 Atoms. *The Journal of Physical Chemistry A* **1997**, *101*, 5111–5116.

(45) Jimenez-Izal, E.; Alexandrova, A. N. Computational design of clusters for catalysis. *Annual review of physical chemistry* **2018**, *69*, 377–400.

(46) Zhai, H.; Alexandrova, A. N. Fluxionality of Catalytic Clusters: When It Matters and How to Address It. *ACS Catalysis* **2017**, *7*, 1905–1911.

(47) Ghosh, P.; Farnesi Camellone, M.; Fabris, S. Fluxionality of Au clusters at ceria surfaces during CO oxidation: Relationships among reactivity, size, cohesion, and surface defects from DFT simulations. *The Journal of Physical Chemistry Letters* **2013**, *4*, 2256–2263.

(48) Zhai, H.; Alexandrova, A. N. Ensemble-average representation of Pt clusters in conditions of catalysis accessed through GPU accelerated deep neural network fitting global optimization. *Journal of chemical theory and computation* **2016**, *12*, 6213–6226.

(49) Sun, G.; Sautet, P. Metastable structures in cluster catalysis from first-principles: Structural ensemble in reaction conditions and metastability triggered reactivity. *Journal of the American Chemical Society* **2018**, *140*, 2812–2820.

(50) Sun, G.; Alexandrova, A. N.; Sautet, P. Structural rearrangements of subnanometer Cu oxide clusters govern catalytic oxidation. *ACS Catalysis* **2020**, *10*, 5309–5317.

(51) Deshpande, S.; Maxson, T.; Greeley, J. Graph theory approach to determine configurations of multidentate and high coverage adsorbates for heterogeneous catalysis. *npj Computational Materials* **2020**, *6*, 1–6.

(52) Kresse, G.; Hafner, J. Ab initio molecular dynamics for liquid metals. *Physical Review B* **1993**, *47*, 558.

(53) Kresse, G.; Hafner, J. Ab initio molecular-dynamics simulation of the liquid-metal–amorphous-semiconductor transition in germanium. *Physical Review B* **1994**, *49*, 14251.

(54) Kresse, G.; Furthmüller, J. Efficient iterative schemes for ab initio total-energy calculations using a plane-wave basis set. *Physical review B* **1996**, *54*, 11169.

(55) Kresse, G.; Furthmüller, J. Efficiency of ab-initio total energy calculations for metals and semiconductors using a plane-wave basis set. *Computational materials science* **1996**, *6*, 15–50.

(56) Perdew, J. P.; Burke, K.; Ernzerhof, M. Generalized gradient approximation made simple. *Physical review letters* **1996**, *77*, 3865.

(57) Blöchl, P. E. Projector augmented-wave method. *Physical review B* **1994**, *50*, 17953.

(58) Kresse, G.; Joubert, D. From ultrasoft pseudopotentials to the projector augmented-wave method. *Physical review b* **1999**, *59*, 1758.

(59) Behler, J. Atom-centered symmetry functions for constructing high-dimensional neural network potentials. *The Journal of chemical physics* **2011**, *134*, 074106.

(60) Bartók, A. P.; Kondor, R.; Csányi, G. On representing chemical environments. *Physical Review B* **2013**, *87*, 184115.

(61) Huo, H.; Rupp, M. Unified representation of molecules and crystals for machine learning. *arXiv preprint arXiv:1704.06439* **2017**,

(62) Behler, J.; Parrinello, M. Generalized Neural-Network Representation of High-Dimensional Potential-Energy Surfaces. *Phys. Rev. Lett.* **2007**, *98*, 146401.

(63) Gastegger, M.; Schwiedrzik, L.; Bittermann, M.; Berzsenyi, F.; Marquetand, P. wACSF—Weighted atom-centered symmetry functions as descriptors in machine learning potentials. *The Journal of chemical physics* **2018**, *148*, 241709.

(64) Singraber, A.; Morawietz, T.; Behler, J.; Dellago, C. Parallel multistream training of high-dimensional neural network potentials. *Journal of chemical theory and computation* **2019**, *15*, 3075–3092.

(65) Wales, D. J.; Doye, J. P. Global optimization by basin-hopping and the lowest energy structures of Lennard-Jones clusters containing up to 110 atoms. *The Journal of Physical Chemistry A* **1997**, *101*, 5111–5116.

(66) Gehrke, R.; Reuter, K. Assessing the efficiency of first-principles basin-hopping sampling. *Physical Review B* **2009**, *79*, 085412.

(67) White, R. P.; Mayne, H. R. An investigation of two approaches to basin hopping minimization for atomic and molecular clusters. *Chemical physics letters* **1998**, *289*, 463–468.

(68) Kim, H. G.; Choi, S. K.; Lee, H. M. New algorithm in the basin hopping Monte Carlo to find the global minimum structure of unary and binary metallic nanoclusters. *The Journal of chemical physics* **2008**, *128*, 144702.

(69) https://github.com/vsumaria/Pt_CO_steps_NNP.